Heliyon 6 (2020) e03588

Contents lists available at ScienceDirect

Heliyon

journal homepage: www.cell.com/heliyon

Research article

Effect of Ni doping on structure, morphology and opto-transport properties of spray pyrolised ZnO nano-fiber

M. Younus Ali [a], M.K.R. Khan [a,*], A.M.M. Tanveer Karim [b], M. Mozibur Rahman [a], M. Kamruzzaman [c]

[a] Department of Physics, University of Rajshahi, Rajshahi-6205, Bangladesh
[b] Department of Physics, Rajshahi University of Engineering and Technology, Rajshahi-6204, Bangladesh
[c] Department of Physics, Begum Rokeya University, Rangpur, Rangpur 5400, Bangladesh

ARTICLE INFO

Keywords:
Materials science
Thin films
Semiconductor
Band gap
Activation energy

ABSTRACT

Nano-fiber structure of ZnO and Ni doped ZnO (Ni:ZnO) transparent thin films have been deposited on glass substrate at 350 °C at an ambient atmosphere via spray pyrolysis technique. The structural, surface morphological and opto-electrical properties of ZnO and Ni doped ZnO thin films have been investigated. The XRD patterns show that the films are of polycrystalline in nature having preferential orientation (0 0 2) plane for ZnO changes to (1 0 1) by Ni doping in ZnO matrix. Optical study exhibits red shifting in band gap energy with Ni doping due to *sp-d* hybridization and display high absorption coefficient of the order of 10^7 m^{-1}. The photoluminescence (PL) spectra indicate blue emissions in all samples. Electrical measurement confirms the resistivity of the film decreases remarkably with Ni doping and electrical transport is mainly thermally activated. From Hall Effect study, it is confirmed that all the samples are n-type having carrier concentration of the order of 10^{18} cm^{-3}. Both mobility and carrier concentrations of the films became higher than ZnO sample with the increase of Ni concentration.

1. Introduction

Transparent conducting oxide (TCO) thin films based on zinc oxide (ZnO) have received much interest because of relatively inexpensiveness compared to indium tin oxide (ITO). ZnO is a multifunctional II-VI group semiconductor which creating a center of attention to researchers because of its fascinating properties such as wide band gap of 3.37 eV at room temperature, large exciton binding energy (60 meV), high optical transparency, high surface stability, large electrochemical coupling coefficient and strong excitonic emission etc (Dehkordi et al., 2019; Luo et al., 2019; Gandhi et al., 2019; Karim et al., 2015a, 2016). Although, stoichiometric ZnO is an insulator, it exists as an n-type semiconductor partially due to its deviation from stoichiometry i.e., due to the presence of interstitial Zn atoms (Zn_i) in large voids and the presence of oxygen vacancies (V_o) in the crystal lattice and partially due to the presence of background donors such as H and Al (Joseph et al., 1999). These defects form donor levels below the conduction band at about 0.05 eV. The interest is growing on ZnO due to its potential applicability in solar cells (Consonni et al., 2019), light-emitting diodes (Rahman, 2019), piezoelectric devices (Kumar et al., 2019), Ultraviolet (UV) photo detectors (Ning et al., 2018; Zhang et al., 2019), antibacterial activities (Hajiashrafi and Kazemi, 2019) and gas sensors (Ganesh et al., 2017; Dewan et al., 2018). On the other hand, Nickel (Ni) is a transition metal element which belongs to the 4^{th} period and 10^{th} group in the periodic Table along with Iron (Fe) and Cobalt (Co). It is known that the transition metals slowly lose their strong metallic characteristics. Nickel is a good conductor of heat and electricity. However, it loses its metallic character very slowly. The most important oxidation state of nickel is +2, although the +3 and +4 oxidation states are also known (Tundermann et al., 2005). Nickel has a relatively average electro negativity that indicates a decent affinity for bonding with other elements. The ionic radii of Ni^{2+} (0.69 Å) and Zn^{2+} (0.74 Å) are very close and they have same valance with same structure (Aboud et al., 2019). It is expected that Ni^{2+} can be easily replaced by Zn^{2+} in ZnO lattice without changing the hexagonal structure of ZnO. Therefore, Ni doped ZnO thin films may effectively be a promising material for obtaining a very good electrical, opto-electronic, thermal and visible luminescence properties.

* Corresponding author.
E-mail address: fkrkhan@yahoo.co.uk (M.K.R. Khan).

https://doi.org/10.1016/j.heliyon.2020.e03588
Received 29 August 2019; Received in revised form 19 January 2020; Accepted 10 March 2020

There are many reports for Ni doped ZnO thin films deposition and characterization, such as by spin coating (Yildiz et al., 2011), sol-gel immersion (Ismail et al., 2018), magnetron sputtering (Bayram et al., 2019) and spray pyrolysis technique (Ali et al., 2020; Owoeye et al., 2019; khalidi et al., 2019; İskenderoğlu and Güney, 2017; Rouchdi et al., 2017; Rajeh et al., 2016). Most of the cases, electrical properties of Ni:ZnO thin films are found inconsistent with Ni doping concentration and the optical properties such as transmittance and band gap are incoherent with Ni doping. Rouchdi et al. (2017) report a controvertal result that the band gap of ZnO increases with the increase of Ni doping. Moreover, M. Rouchdi et al. and A. Yildiz et al. (Rouchdi et al., 2017; Yildiz et al., 2011) also report that the electrical conductivity of ZnO decreases significantly with the increase of Ni doping which makes a conflict with concept of Ni doping. Because it is logically expected that the reduction of resistivity with Ni replacing Zn site as Ni is a good metal and very insignificant mismatching of ionic radius between Zn^{2+} and Ni^{2+} ions induces low lattice distortion. Furthermore, another debatable report published by Rajeh et al. (2016) in which they claim that the crystal growth plane of ZnO does not change with Ni-doping. However, elemental doping may change crystal habit plane for ZnO doping with (Cu, N) as reported by Liton et al., (2015). Therefore, there are still many controversies remains in experimental results and explanation of physics.

Considering the immense applications of ZnO in the field of opto-electronic, we motivated to prepare ZnO and Ni doped ZnO thin films by a simple low cost spray-pyrolysis (SP) technique. It is our aim to study the effect of Ni doping on its structural, optical and electrical properties and to explore physics which may be helpful for the applications in the field of opto-electronic devices.

2. Experimental techniques

ZnO and Ni doped ZnO (Ni:ZnO) thin films were deposited on glass substrate using spray pyrolysis technique at an ambient atmosphere. The details of film preparation and optimization process for obtaining a good quality film by spray pyrolysis are given elsewhere (Shah et al., 2018). The working solution was prepared by mixing the appropriate amounts of 0.1 M zinc acetate dihydrate ($(CH_3COO)_2Zn.2H_2O$) and nickel chloride hexahydrate ($NiCl_2.6H_2O$) dissolved with in de-ionized water. Zinc acetate and nickel chloride were mixed together in different nominal volume ratios to obtain 0, 1.0, 2.0, 4.0 and 6.0 mol% Ni doped ZnO thin films. The solution flow rate and gas pressure were kept constant at 0.5 ml/min and 2.5 psi, respectively. The distance between spray nozzle and substrate was kept at 0.20 m, spraying time was 15 min. The substrate temperature was kept at ~ 350 °C measured by a copper-constantan thermocouple. The possible chemical reactions that take place on the heated substrate to produce ZnO and Ni doped ZnO thin films may be as follows:

$$Zn(CH_3COO)_2.2H_2O \xrightarrow[\text{Decomposes to}]{350^\circ C} ZnO + CO_2(g) + CH_4(g) + \text{Steam}(g)$$

$$(CH_3COO)_2Zn.2H_2O + NiCl_2.6H_2O \xrightarrow[\text{Decomposes to}]{350^\circ C} ZnO{:}Ni + CO_2(g) + Cl_2(g) + CH_4(g) + \text{Steam}(g)$$

Thin film growth parameters were kept constant for all Zn/Ni ratios to obtain same thickness of the films. The thickness of the films was measured by Newton's ring method and found to be ~ (180 ± 10) nm.

The crystallographic structure of the pure ZnO and Ni:ZnO films was studied by a X-ray diffractometer D2 PHASER (BRUKER). The diffraction profile of all samples was recorded in between Bragg angle of (20–70)° with Cuk_α monochromatic radiation of wavelength $\lambda = 0.15405$ nm, tube current 10 mA, voltage 30 kV and in steps of 0.02°.The surface morphology of ZnO and Ni:ZnO films were studied by scanning electron microscope (SEM) (Philips XL30 FEG). Optical transmittance and reflectance data were taken using a UV-visible spectrophotometer (UV-1601 PC SHIJMADZU). The room temperature photoluminescence (RTPL) measurement was performed using a spectrofluorophotometer (RF-5301, Shimadzu, Japan) at an excitation wavelength of 370 nm. Hall voltage and resistivity measurements were carried out by van der Pauw's method using a Keithley electrometer.

3. Results and discussion

3.1. Structural analysis

The crystal structure of the deposited films was determined using high-resolution X-ray diffractometer at room temperature. The XRD patterns of ZnO and Ni doped ZnO films are shown in Figure 1. From figure it is observed that the films are of polycrystalline in nature. It is also clear from XRD patterns that no impurity phase is present in the ZnO samples. The characteristic peak positions are identified comparing with JCPDS card no 89–1397. The characteristic peaks are at 2θ = 31.94°, 34.52°, 36.41°, 47.55°, 56.77°, 62.82°, 68.00° corresponding to (h k l) values of (1 0 0), (0 0 2), (1 0 1), (1 0 2), (1 1 0), (2 0 0), (1 1 2), respectively.

From the analysis of XRD peak positions, ZnO and Ni doped ZnO samples could be indexed with hexagonal (wurtzite) structure. The XRD patterns also revealed that the films are in good crystalline and the crystallites of the samples are oriented in different planes. The dominant peak positions are observed at *2θ* values of 31.94°, 34.52° and 36.41° on the other hand the minor peaks are at 47.55°, 56.77°, 62.82° and 68.00°. It is also observed that the intensity of (0 0 2) reflection is maximum for ZnO and 1 mol% Ni:ZnO films, which indicates that ZnO and 1 mol% Ni:ZnO films have preferential orientation in the (0 0 2) plane. While the preferential orientation of 2, 4 and 6 mol% Ni:ZnO thin films changes to (1 0 1) plane and no other secondary phases of Ni or its oxides are seen within the scanning range suggesting that Ni substitutes Zn sites in ZnO lattice. S.K. Mandal et al. and M. Kamruzzaman et al. reported that the solubility limits of Ni into ZnO is very low at temperature ≥100 °C, however, it is increased with the increase of growth temperature (Mandal et al., 2006; Kamruzzaman and Zapien, 2017). In this work, film growth

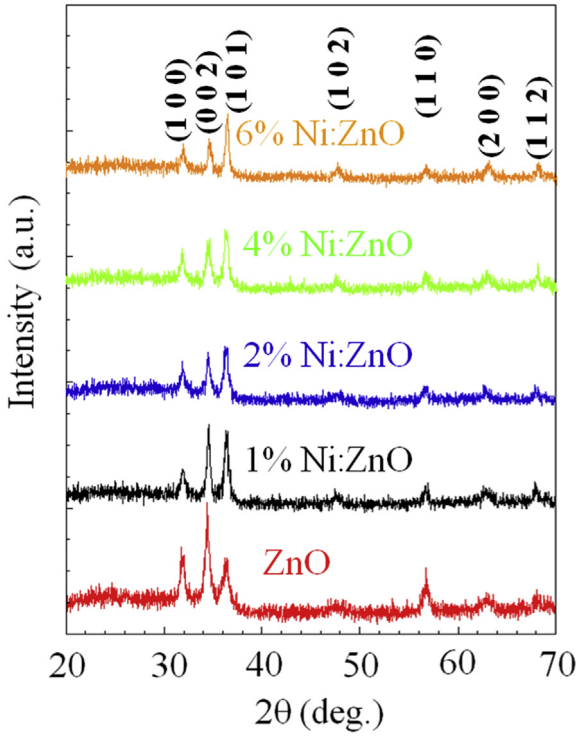

Figure 1. X-ray diffraction patterns of ZnO and Ni doped ZnO thin films.

temperature was 350 °C and the solubility is higher which was expected and confirmed as there is no impurity phases present in the XRD patterns.

Comparing the observed diffraction peak positions and relative intensity with the standard value of ZnO lattice (JCPDS card no.89–1397) the d_{hkl} values of ZnO and Ni doped ZnO were calculated using the Bragg's law:

$$2\, d_{hkl} \sin\theta = n\lambda \quad (1)$$

where, d_{hkl} is the inter-planer spacing, θ is the Bragg angle and λ is the wavelength of radiation. The calculated values of average lattice parameters, d_{hkl} for all samples are given in Table 1. The size of the grown crystallites was estimated by using the Debye-Scherrer formula (Cullity and Stock, 2001):

$$\xi = \frac{0.94\,\lambda}{\beta cos\theta} \quad (2)$$

where, ξ is the crystallite size, λ is the wavelength of the X-ray used, θ is the diffraction angle and β is the full width at half maximum (FWHM) measured in radians.

The corresponding lattice strain, ε was calculated by using the following relation (Ashaduzzman et al., 2018):

$$\varepsilon = \frac{\beta}{4\tan\theta} \quad (3)$$

The dislocation density (δ) of the samples was estimated using the equation (Ashaduzzman et al., 2018):

$$\delta = \frac{1}{\xi^2} \quad (4)$$

The calculated crystallite size or grain sizes, lattice constants, dislocation densities and strain for (1 0 1) plane are given in Table 1. A very small change in lattice parameters was observed due to the doping because of small difference in ionic radius between Zn^{2+} and Ni^{2+}. The lattice constant *a* remains more or less unchanged but *c* slightly decreases with increasing doping concentration of Ni. This may be happened due to changes of preferential orientation with Ni doping concentration and since the ionic radius of Ni is slightly smaller that of Zn ion. From the Table 1, it is observed that the crystallite size of Ni:ZnO samples increases, whereas, strain and dislocation decreases with doping concentration of Ni. The reduction of strain and dislocation density may be attributed to the improved crystallinity of the film due to decrease of lattice misfit in the film. However, the grain size of 4 mol % Ni doped sample is found lower subsequently strain and dislocation density increases compare to other doped samples because of the strain and dislocation density are inversely related to the grain size. There are many factors affecting micro-structure of crystallite during crystal growth. In this case it seems thermodynamic instability during crystal growth perturbed (1 0 1) plane crystallization resulting in reduction of crystal size subsequently increase of strain and dislocation density for 4 mol% Ni doped sample. The increase of strain and dislocation density due to Ni doping is reported by İskenderoğlu et al. (İskenderoğlu and Güney, 2017).

3.2. Surface morphology

The SEM micrographs of ZnO and Ni:ZnO thin films at different magnifications are shown in Figure 2(a-e). The SEM indicates that the surface of substrate is well covered by nanostructure and the deposition led to number of clusters with well-defined nucleation centers. The clusters consist of highly dense ganglia-like fibers over a large area around the nucleation centers. The fibers of different lengths and cross-sections are oriented randomly, because these nano-fibers were produced by self assembly process with low level super-saturation of reactants. The anisotropy of wurtzite ZnO structure may also enhances the nano-fiber growth by terminating the basal polar plane in between positive (Zn^{2+}, Ni^{2+}) and negative (O^{2-}) lattice points. Such nano-fiber growth of ZnO and Ni:ZnO have also been reported (Qiao et al., 2013; Das et al., 2013). The nano-structured surfaces of all samples are found almost same except the density of the nano-fiber varies from film to film with different doping concentration of Ni in ZnO. In general, the formation of self assembled nano structure depends on thermodynamic environment and crystal growth parameters. In this work, we have used identical growth parameters at constant temperature for all samples. Furthermore, the crystallization behavior of ZnO is supposed to not influence very much by Ni doping because of the similar crystal structure and radii of Ni^{2+} and Zn^{2+}. As a result, Ni:ZnO nano fibers are similar as pristine ZnO nano fiber.

3.3. Optical study

The optical transmission T(λ) and reflection R(λ) spectra of ZnO and Ni:ZnO thin films are shown in Figure 3. It is seen from Figure 3 (left scale) that the transmittance increases sharply in the lower wavelength (380 nm–420 nm) region and becomes nearly flat in the higher wavelength (500 nm–1100 nm) region.

A sharp decrease in the transmittance is observed at ~380 nm attributed to the band edge absorption and the transition is direct. This strong absorption means that the incoming photons have the sufficient energy to excite electrons from the valence band to the conduction band (Farag et al., 2011). Maximum value of transmittance (~75%) was obtained for ZnO thin film and then gradually decreases with increasing doping concentration of Ni which is in good agreement with the reported results (Ghosh et al., 2008). A small red shift is observed at the band edge absorption with the increase of Ni doping suggesting the band gap reduction occurred due to the increase of Ni doping. In addition, a small damping of absorption is observed at wavelength ~670 nm (indicated by an arrow sign) for Ni doped ZnO sample. The appearance of this absorption becomes distinct for higher doping level of Ni. This absorption is a typical characteristic of *d-d** intra-ionic transitions in the tetrahedral coordinate of high-spin Ni^{2+} ion. This may be attributed to the transfer of charge carriers in between donor and acceptor ionization levels situated inside the band gap of ZnO lattice (Dinia et al., 2005; Saha et al., 2015) or creation of deep level defect states by the doping of Ni.

From the right scale of Figure 3, it is seen that the reflectance of ZnO thin films gradually decreases with increasing doping concentration of Ni. The energy dependence of the reflectance shows that it initially

Table 1. Data for the value of d_{hkl}, lattice constants, dislocation density (δ), grain size (ζ) and strain (ε) for (1 0 1) plane of ZnO and Ni:ZnO thin films.

Doping con. (mol %)	d_{101} (nm)	Lattice constants		ζ (nm)	δ ×10^{15} (lines/m^2)	ε × 10^{-2} (%)
		a (nm)	*c* (nm)			
0	0.2468	0.3242	0.5206	24	1.73	52
1	0.2467	0.3234	0.5196	37	0.73	36
2	0.2472	0.3240	0.5213	32	0.97	41
4	0.2472	0.3245	0.5203	25	1.60	52
6	0.2468	0.3243	0.5181	37	0.73	36

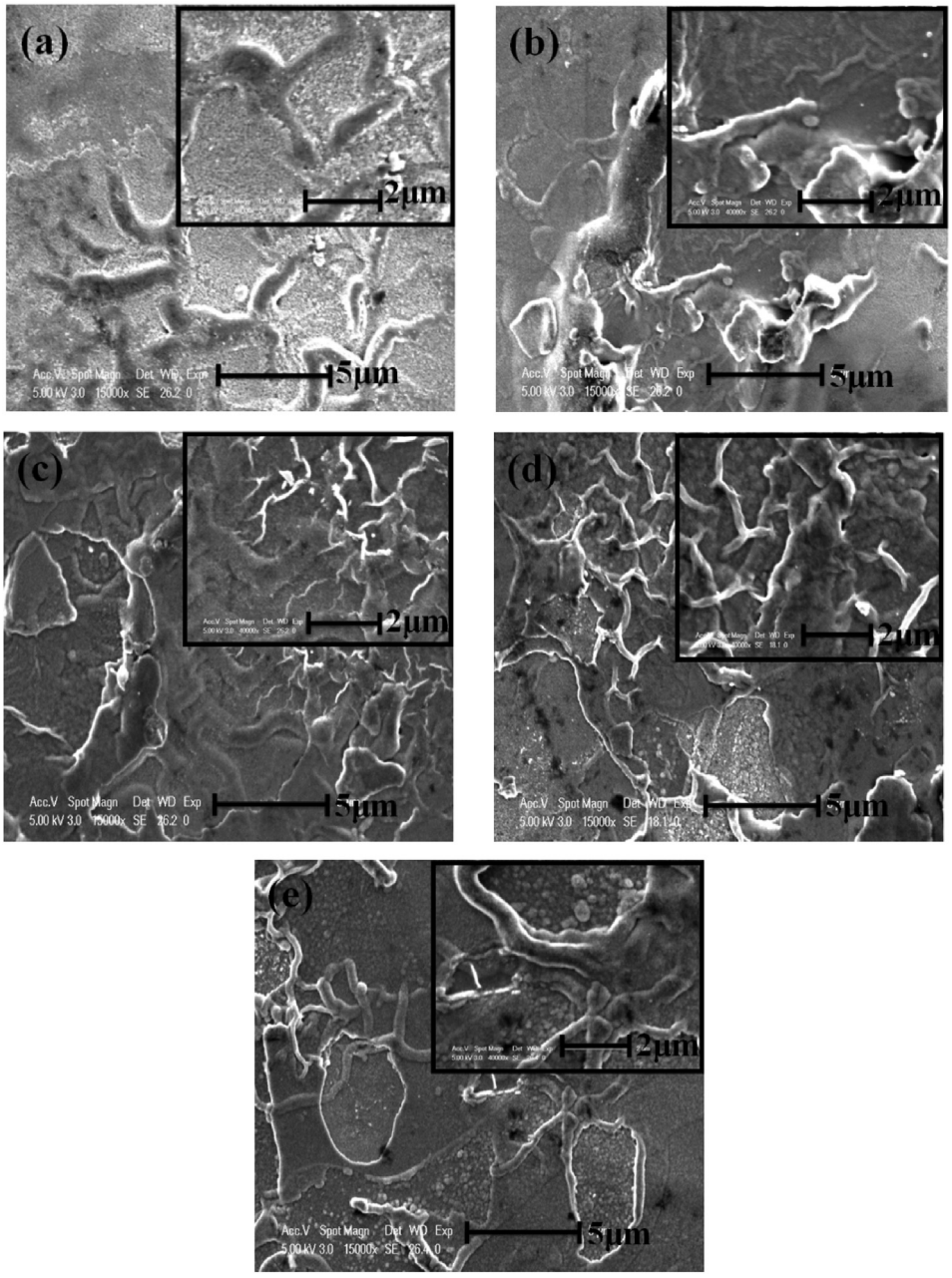

Figure 2. SEM micrographs at magnification of 15000X for (a) ZnO, (b) 1 mo% Ni, (c) 2 mol% Ni, (d) 4 mol% Ni and (e) 6 mol% Ni doped ZnO nano-fibers. Inset shows the SEM images at magnification of 40000X.

increases in the lower wavelength region for ZnO and Ni:ZnO after which decreases up to ~760 nm and then again slightly increases up to ~850 nm. The lower reflectance with increasing doping suggests that doped samples are slightly rough compared to ZnO thin film.

The optical band gap E_g can be determined using optical absorption equation (Mott and Gurney, 1940):

$$\alpha h\nu = A\left(h\nu - E_g\right)^m \tag{5}$$

where A is an energy-independent constant, superscript m determines the nature of transition involved, where, m = 1/2 for direct transition and α is the absorption co-efficient calculated from transmittance and reflectance data using the relation (Karim et al., 2015b, 2019):

$$\alpha = \frac{1}{t} ln\left[\frac{(1-R)^2}{T}\right] \tag{6}$$

The absorption coefficient of the film depends on thickness, impurities and on doping concentration also. The variation of absorption co-efficient with wavelength is shown in Figure 4 which increases slightly with increasing Ni concentration. It is found that the value of absorption coefficient, α is sufficiently high of the order of 10^7 m^{-1}.

The variation of $(\alpha h\nu)^2$ (direct allowed transition) with hν for ZnO and Ni:ZnO thin films are shown in Figure 5.

The band gap energy was obtained from the intercept on the energy axis after extrapolation of the straight line section of the curves and the obtained values are tabulated in Table 2. From the Table 2, it is found

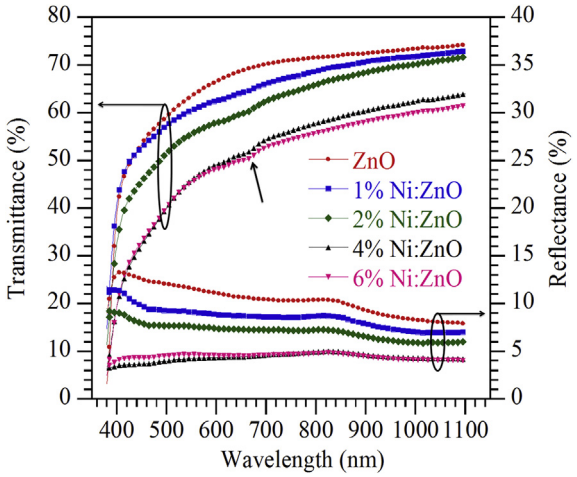

Figure 3. Variation of transmittance (left scale) and reflectance (right scale) with wavelength for ZnO and Ni doped ZnO thin films.

that the band gap shows a red shift from 3.20 to 3.13 eV with the increase of Ni concentration from 0 to 6 mol%. The band gap values of ZnO and Ni:ZnO is slightly lower but the tendency of decreasing band gap with Ni doping is consistent with previously published reports (Ali et al., 2020; Owoeye et al., 2019; İskenderoğlu and Güney, 2017; Rajeh et al., 2016). A comparison of band gap between this work and previously reported work (İskenderoğlu and Güney, 2017) is given in Table 2.

This reduction of the band gap energy indicates the incorporation of Ni affects the optical band gap. The small reduction of the band gap energy (~0.07 eV) can be interpreted in terms of the *sp-d* exchange interaction of the direct coupling between the band electron spin O_{bes} and magnetic ion spin S_{mis} forming $-JO_{bes}.S_{mis}$ (Kossut, 1976; Bastard et al., 1977; Kamruzzaman et al., 2012) and the *sp-d* hybridization occurs between the host valance band conduction electron and the impurity magnetic ions (Kim et al., 1993). However, the direct exchange interaction in Ni:ZnO system has much smaller effect on the band gap energies than the *sp-d* hybridization interaction (Kim et al., 1993). When Ni^{2+} ion is added to ZnO, the 3d levels of impurity Ni^{2+} ions exists below the conduction band of ZnO and constitutes the *sp-d* hybridization. In this study the small reduction of band gap energy with increasing Ni concentration in ZnO may be caused by decreasing *sp-d* hybridization energy which results in the reduction of band gap energy.

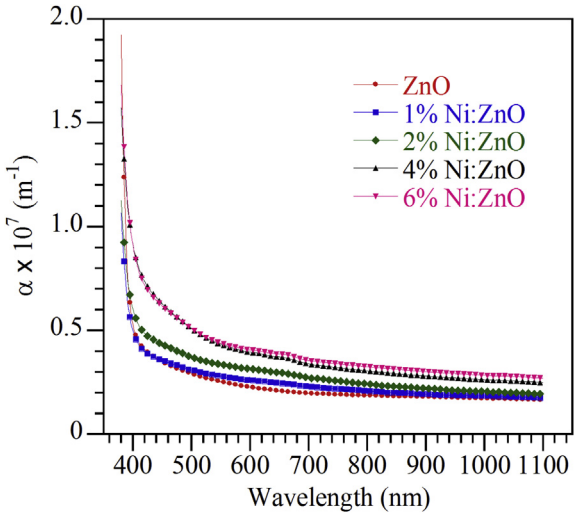

Figure 4. Variation of absorption coefficient with wavelength for ZnO and Ni doped ZnO thin films.

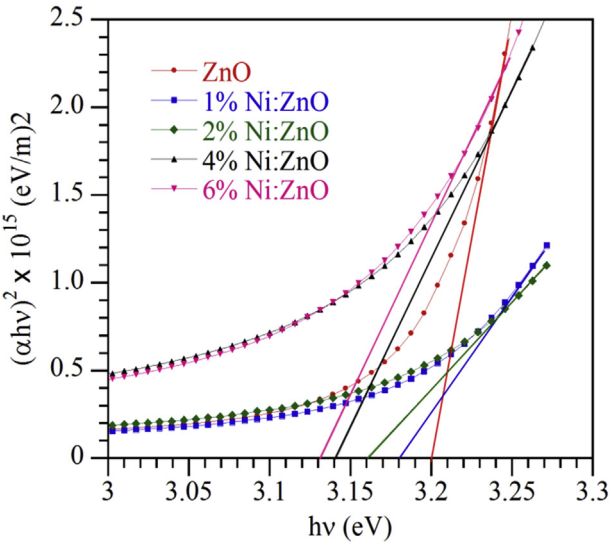

Figure 5. Variation of $(\alpha h\upsilon)^2$ with photon energy for ZnO and Ni doped ZnO thin films.

3.4. Photoluminescence (PL) study

The intensity of the photoluminescence signal provides information of the quality of surface of the film. The room temperature photoluminescence (RTPL) spectra were taken in the wavelength range 420 nm–550 nm. The variation of photoluminescence intensity with wavelength for ZnO and Ni:ZnO thin films at an excitation energy 3.37 eV (λ = 370 nm) is shown in Figure 6 (a).

From Figure, it is seen that the PL peaks of ZnO and Ni:ZnO samples are almost in the same position but have different intensities. The origin of the entire PL emissions lie within the wavelength range (450–490) nm may be explained by an energy level diagram given in Figure 6 (b). From figure it is clear that the blue emissions originated from the recombination of trapped holes and electrons at Zn vacancies (V_{Zn}) and Zn interstitial (Zn_i), respectively, and the recombination of trapped electrons at Zn_i sites with photo generated holes (Ali et al., 2020; Zeng et al., 2010). Theoretical calculations predict that V_{Zn} and Zn_i can create easily in ZnO matrix because of their lower formation energy (Zeng et al., 2010; Kavitha et al., 2014). The non-equilibrium processes of thin film growth and doping may also induce the defect formation which causes deep energy levels in the band gap. In general, Zn_i act as a shallow donor levels and V_{Zn} produces acceptor levels. The emission bands observed at around 452 nm (2.75 eV) may be caused by the electron transition from the energy level of Zn_i site to the top of valance band (VB) (Farag et al., 2011; Fang et al., 2004; Zeng et al., 2010), whereas, the peaks at 470 nm (2.65 eV) and 485 nm (2.56 eV) are originated by electron transitions in between the bottom of the conduction band (CB) and acceptor V_{Zn} site (Ali et al., 2020; Zeng et al., 2010; Kavitha et al., 2014).

3.5. Transport properties

The resistivity of the ZnO and Ni:ZnO thin films was measured by the Van-der Pauw's method from RT to 455 K. During each measurement, temperature was increased slowly to ensure that the film was at uniform temperature. The variation of resistivity with temperature is shown in Figure 7.

It is observed that the resistivity for all samples gradually decrease with increasing temperature which is the signature of semiconducting nature with negative temperature coefficient of resistance (TCR). Figure 7 also reveals that the resistivity of ZnO thin film (Inset of Figure 7) has two steps, first it decreases sharply in the low temperature region (300–340) K, after that it decreases slowly with temperature. This

Table 2. Values of direct band gap energy (E_g), Hall mobility (μ_H), carrier concentration (n_c), RT resistivity (ρ) and activation energy (ΔE) of ZnO and Ni:ZnO thin films.

Doping (mol %)	E_g (eV)		μ_H (cm^2/Vsec)		$n_c \times 10^{18}$ (cm^{-3})		$\rho \times 10^{-2}$ (Ω-cm^{-1})		ΔE (eV)	
	This work	İskenderoğlu and Güney (2017)	This work	Rouchdi et al. (2017)	This work	Rouchdi et al. (2017)	This work	Rouchdi et al. (2017)	ΔE_1 (310–330) K	ΔE_2 (405–435) K
0	3.20	3.27	4.70	4.6	2.34	51.2	57	2.65	0.071	0.239
1	3.18	3.25	36.73	-	6.09	-	2.80	-	0.168	0.226
2	3.16	3.25	37.01	5.7	7.53	95.3	2.24	1.15	0.188	0.316
4	3.14	3.19	35.49	6.31	8.14	49.2	2.16	2.01	0.269	0.285
6	3.13	-	55.39	8.15	8.80	25.8	1.28	2.97	0.242	0.696

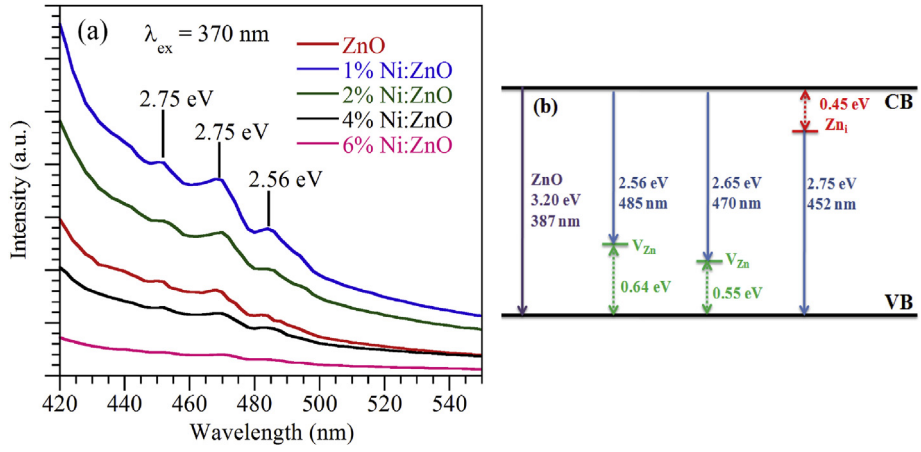

Figure 6. (a) Room temperature photoluminescence spectra of ZnO and Ni doped ZnO thin films, (b) A probable energy level diagram of PL emissions due to defects.

is due to more activation energy of donor transition required at low temperature than that of high temperature. The resistivity decreases in a regular fashion with the increasing doping concentration of Ni. It should be noted that the RT resistivity is significantly lower for Ni doped samples than un-doped ZnO. The reduction in resistivity due to doping is understandable, as some Zn atoms with full *3d* shells (providing only semi core valance band states) are replaced with Ni, where the *3d* shell is not full ($3d^8$) and has states near the bottom of the conduction band. This addition of conduction band states will accommodate more conduction electrons and therefore lower the resistivity (Das et al., 2013). The room temperature resistivity of ZnO and Ni:ZnO is given in Table 2 and compared with previous work (Rouchdi et al., 2017).

To calculate the activation energy of ZnO and Ni:ZnO thin films, the variation of lnσ versus inverse temperature is plotted shown in Figure 8. The activation energy may be obtained by using the relation

$$\sigma = \sigma_0 \exp\left(-\frac{\Delta E}{2K_B T}\right) \tag{7}$$

where ΔE is the activation energy, K_B is the Boltzmann constant, σ is the electrical conductivity and σ_o is the pre-exponential factor. From the slope of lnσ vs. 1/T plot, the activation energy ΔE_1 was calculated at (310–330) K and ΔE_2 at (405–435) K. The values of ΔE_1 and ΔE_2 are given in Table 2. From the Table 2, it is observed that the activation energy ΔE_2 is higher than that of ΔE_1. The high values indicate that

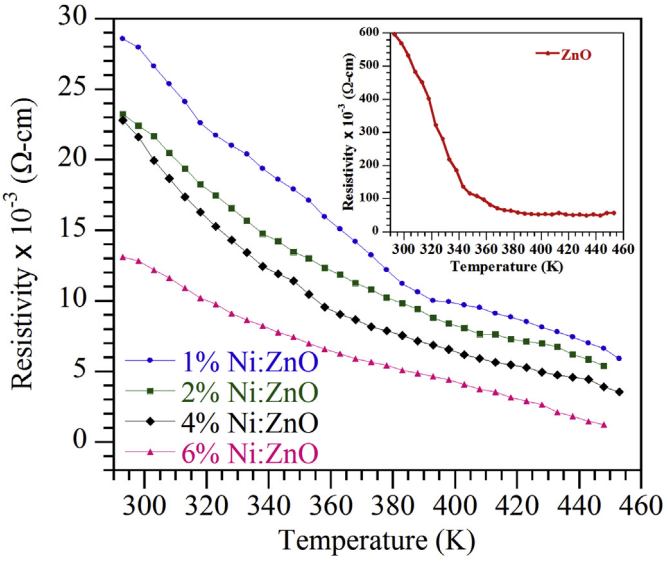

Figure 7. Variation of resistivity with temperature for Ni doped ZnO thin films. The inset shows the variation for ZnO film.

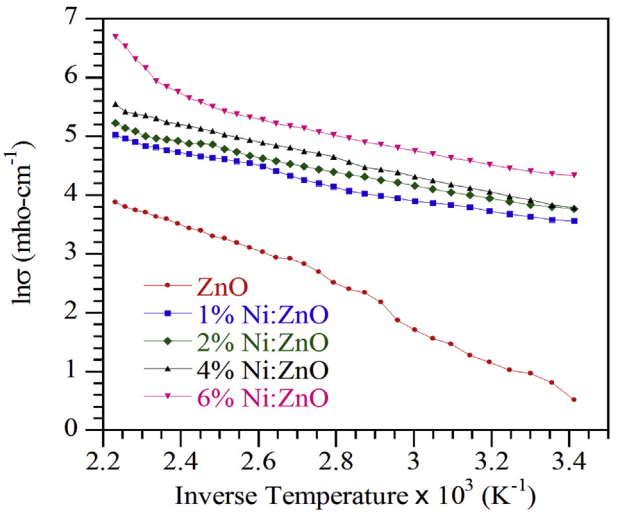

Figure 8. Variation of lnσ with inverse temperature for ZnO and Ni doped ZnO thin films.

conductivity is associated with the free band transition of carriers i.e. from donor level to conduction band and the low values of ΔE_1 may be associated with the localized levels hopping due to the excitation of carriers from one defect state to other (Mott and Gurney, 1940). The electron resides at this site until it is thermally activated to migrate to another site (Mott and Gurney, 1940).

The RT Hall effect measurement was done at a constant magnetic field of 9.815 KG. The Hall study confirmed that the carriers of ZnO and Ni:ZnO samples are n-type. From the Hall Effect measurement, Hall mobility (μ_H) and carrier concentration (n_c) have been calculated. The mobility measured in this work is higher but the carrier concentration is found lower compared with previous report (Rouchdi et al., 2017) and tabulated in Table 2. From the table, it is clear that both the carrier concentration and Hall mobility increases with Ni doping concentration and the carrier concentrations of all samples are found in the order of 10^{18} cm^{-3}.

4. Conclusions

In the present work, ZnO and Ni:ZnO thin films were successfully synthesized using low cost spray pyrolysis technique on glass substrate at substrate temperature ~350 °C. XRD patterns showed that the films are mono-phasic and polycrystalline in nature having hexagonal wurtzite structure. The preferential orientation of (0 0 2) plane for ZnO and 1 mol % Ni:ZnO films changes to (1 0 1) plane for 2, 4 and 6 mol% Ni: ZnO films. The SEM micrographs revealed that the surfaces are well covered by nano-fiber like crystal grains. In optical study all samples exhibit high absorption coefficient of the order of 10^7 m^{-1} and the appearance of *d-d** intra-ionic transitions in the tetrahedral coordinate of high-spin Ni^{2+} ion is found for Ni doped samples. The band gap of ZnO is tuned from 3.20 eV to 3.13 eV with increasing Ni doping due to *sp-d* hybridization and exchange parameter. Photoluminescence study confirms blue emissions in all samples. From transport measurements it is found that the conductivity of ZnO remarkably increased with Ni doping. The value of activation energy at higher temperature region is higher than lower temperature region which manifests that at high temperature carrier transportation associated with free band transition and at low temperature it is hopping. Hall effect study confirmed that ZnO and Ni:ZnO films are n-type semiconductor having carrier concentrations of the order of ~10^{18} cm^{-3}. All these observed parameters of nano-fiber like Ni:ZnO films seems suitable for sensing device, laser and photovoltaic applications.

Declarations

Author contribution statement

M. Younus Ali, M.K.R. Khan, A.M.M. Tanveer Karim, M. Mozibur Rahman, M. Kamruzzaman: Conceived and designed the experiments; Performed the experiments; Analyzed and interpreted the data; Wrote the paper.

Funding statement

This research did not receive any specific grant from funding agencies in the public, commercial, or not-for-profit sectors.

Competing interest statement

The authors declare no conflict of interest.

Additional information

No additional information is available for this paper.

Acknowledgements

Authors are thankful to and acknowledging Department of Materials Science and Engineering, City university of Hong Kong for providing XRD and SEM facilities.

References

Aboud, A.A., Shaban, M., Revaprasadu, N., 2019. Effect of Cu, Ni and Pb doping on the photo-electrochemical activity of ZnO thin films. RSC Adv. 9, 7729–7736.
Ali, H., Alsmadi, A.M., Salameh, B., Mathai, M., Shatnawi, M., Hadia, N.M.A., Ibrahim, E.M.M., 2020. Influence of Nickel Doping on the Energy Band gap, Luminescence, and Magnetic order of spray deposited nanostructured ZnO thin films. J. Alloys Compd. 816, 152538.
Ashaduzzman, M., Khan, M.K.R., Karim, A.M.M.T., Rahman, M.M., 2018. Influence of chromium on structural, non-linear optical constants and transport properties of CdO thin films. Surf. Int. 12, 135–144.
Bastard, G., Rigaux, C., Mycielski, A., 1977. Giant spin splitting induced by exchange interactions in $Hg_{1-k}Mn_kTe$ mixed crystals. Phys. Status Solidi B 8, 585–593.
Bayram, O., Sener, E., İgman, E., Onder, S., 2019. Investigation of structural, morphological and optical properties of Nickel-doped Zinc oxide thin films fabricated by co-sputtering. J. Mater. Sci. Mater. Electron. 30, 3452–3458.
Consonni, V., Briscoe, J., Kärber, E., Li, X., Cossuet, T., 2019. ZnO nanowires for solar cells: a comprehensive review. Nanotechnology 30, 362001.
Cullity, B.D., Stock, S.R., 2001. Elements of X ray Diffraction. Prentice Hall, New Jersey.
Das, S.C., Green, R.J., Podder, J., Regier, T.Z., Chang, G.S., Moewes, A., 2013. Band gap tuning in ZnO through Ni doping via spray pyrolysis. J. Phys. Chem. C 117, 12745–12753.
Dehkordi, H.A., Mokhtari, A., Dastafkan, K., Soleimanian, V., 2019. Sol-Gel spin-coating followed by solvothermal synthesis of nanorods-based ZnO thin films: microstructural, optical, and gas sensing properties. J. Electron. Mater. 48, 1258–1267.
Dewan, S., Tomar, M., Kapoor, A.K., Tandon, R.P., Gupta, V., 2018. XPS resolved surface states analysis of ZnO and Ni doped ZnO films for quantum well applications. Ferroelectrics 534, 199–205.
Dinia, A., Schmerber, G., Mény, C., Bohnes, V.P., Beaurepaire, E., 2005. Room-temperature ferromagnetism in $Zn_{1-x}Co_xO$ magnetic semiconductors prepared by sputtering. J. Appl. Phys. 97, 123908.
Fang, Z., Wang, Y., Xu, D., Tan, Y., Liu, X., 2004. Blue luminescent center in ZnO films deposited on silicon substrates. Opt. Mater. 26, 239–242.
Farag, A.A.M., Cavas, M., Yakuphanoglu, F., Amanullah, F.M., 2011. Photoluminescence and optical properties of nanostructure Ni doped ZnO thin films prepared by sol-gel spin coating technique. J. Alloys Compnd. 509, 7900–7908.
Gandhi, A.C., Liao, C.-H., Yeh, W.-L., Huang, Y.-L., 2019. Non-monotonous size-dependent photoluminescence and excitonic relaxations in nanostructured ZnO thin films. RSC Adv. 9, 2180–2188.
Ganesh, R.S., Durgadevi, E., Navaneethan, M., Patil, V.L., Ponnusamy, S., Muthamizhchelvan, C., Kawasaki, S., Patil, P.S., Hayakawa, Y., 2017. Controlled synthesis of Ni-doped ZnO hexagonal microdiscs and their gas sensing properties at low temperature. Chem. Phys. Lett. 689, 92–99.
Ghosh, S., Srivastava, P., Pandey, B., Saurav, M., Bharadwaj, P., 2008. Study of ZnO and Ni-doped ZnO synthesized by atom beam sputtering technique. Appl. Phys. Mater. Sci. Process 90, 765–769.
Hajiashrafi, S., Kazemi, N.M., 2019. Preparation and evaluation of ZnO nanoparticles by thermal decomposition of MOF-5. Heliyon 5, e02152.
Ismail, A.S., Mamat, M.H., Malek, M.F., Saidi, S.A., Yusoff, M.M., Mohamed, R., Md Sin, N.D., Suriani, A.B., Rusop, M., 2018. Structural, optical, and electrical properties of Ni-doped ZnO nanorod arrays prepared via sonicated sol-gel immersion method. AIP Confer. Proceed. 1963, 020029.
İskenderoğlu, D., Güney, H., 2017. Synthesis and characterization of ZnO:Ni thin films grown by spray-deposition. Ceram. Int. 43, 16593–16599.
Joseph, M., Tabata, H., Kawai, T., 1999. p-Type electrical conduction in ZnO thin films by Ga and N codoping. Jpn. J. Appl. Phys. 38, L1205–L1207.
Kamruzzaman, M., Zapien, J.A., 2017. Effect of Co and Ni on $Au/Zn_{1-x}M_xO$ nanorods (M = Co and Ni) Schottky photodiodes performance. J. Nanosci. Nanotechnol. 17, 5342–5351.
Kamruzzaman, M., Luna, T.R., Podder, J., Anowar, M.G.M., 2012. Synthesis and characterization of $Cd_{1-x}Co_xS$ thin films prepared using the spray pyrolysis technique. Semicond. Sci. Technol. 27, 035017.
Karim, A.M.M.T., Rahman, M.M., Shahjahan, M., Khan, M.K.R., 2015a. Study of the morphology, photoluminescence and photoconductivity of ZnO-CdO nanocrystals. Mater. Res. Express 2, 036402.
Karim, A.M.M.T., Khan, M.K.R., Rahman, M.M., 2015b. Structural and opto-electrical properties of pyrolized ZnO-CdO crystalline thin films. J. Semiconduct. 36, 053001.
Karim, A.M.M.T., Khan, M.K.R., Rahman, M.M., 2016. Effect of Zn/Cd ratio on the optical constants and photo conductive gain of ZnO-CdO crystalline thin films. Mater. Sci. Semicond. Process. 41, 184–192.
Karim, A.M.M.T., Hossain, M.S., Khan, M.K.R., Kamruzzaman, M., Rahman, M.A., Rahman, M.M., 2019. Solution-processed mixed halide $CH_3NH_3PbI_{3-x}Cl_x$ thin films prepared by repeated dip coating. J. Mater. Sci. 54, 11818–11826.
Kavitha, M.K., Jinesh, K.B., Philip, R., Gopinath, P., John, H., 2014. Defect engineering in ZnO nanocones for visible photoconductivity and nonlinear absorption. Phys. Chem. Chem. Phys. 16, 25093–25100.

Khalidi, Z.E., Hartiti, B., Siadat, M., Comini, E., Arachchige, H.M.M.M., Fadili, S., hevenin, P., 2019. Acetone sensor based on Ni doped ZnO nanostructues: growth and sensing capability. J. Mater. Sci.: Mater. Electron. 30, 7681–7690.

Kim, Y.D., Chang, Y.C., Klein, M.V., 1993. Effect of delectrons in transition-metal ions on band-gap energies of diluted magnetic semiconductors. Phys. Rev. B 48, 17770.

Kossut, J., 1976. Electron transport phenomena in narrow and zero-gap semiconductors containing magnetic impurities. Phys. Status Solidi B 78, 537–542.

Kumar, A., Prasad, M., Janyani, V., Yadav, R.P., 2019. Fabrication and annealing temperature optimization for a piezoelectric ZnO based MEMS acoustic sensor. J. Electron. Mater. 48, 5693–5701.

Liton, M.N.H., Khan, M.K.R., Rahman, M.M., Islam, M.M., 2015. Effect of N and Cu doping on structure, surface morphology and photoluminescence properties of ZnO thin films. J. Sci. Res. 7, 23–34.

Luo, C.-Q., Ling, C.-C.,F., Rahman, M.A., Phillips, M., Ton-That, C., Liao, C., Shih, K., Lin, J., Tam, H.W., Djurišić, A.B., Wang, S.-P., 2019. Surface polarity control in ZnO films deposited by pulsed laser deposition. Appl. Sur. Sci. 483, 1129–1135.

Mandal, S.K., Das, A.K., Nath, T.K., Karmakar, D., 2006. Temperature dependence of solubility limits of transition metals (Co, Mn, Fe, and Ni) in ZnO nanoparticles. Appl. Phys. Lett. 89, 144105.

Mott, N.F., Gurney, R.W., 1940. Electronic Processes in Ionic Crystals. Oxford University Press, London.

Ning, Y., Zhang, Z., Teng, F., Fang, X., 2018. Novel transparent and self-powered UV photodetector based on crossed ZnO nanofiber array homojunction. Small 14, 1703754.

Owoeye, V.A., Ajenifuja, E., Adeoye, E.A., Osinkolu, G.A., Popoola, A.P., 2019. Microstructural and optical properties of Ni-doped ZnO thin films prepared by chemical spray pyrolysis technique. Mater. Res. Express 6, 086455.

Qiao, L., Wang, X., Sun, X., Li, X., Zheng, Y., He, D., 2013. Single electrospun porous NiO-ZnO hybrid nanofibers as anode materials for advanced lithium-ion batteries. Nanoscale 5, 3037–3042.

Rahman, F., 2019. Zinc oxide light-emitting diodes: a review. Opt. Eng. 58, 010901.

Rajeh, S., Barhoumi, A., Mhamdi, A., Leroy, G., Duponchel, B., Amlouk, M., Guermazi, S., 2016. Structural, morphological, optical and opto-thermal properties of Ni-doped ZnO thin films using spray pyrolysis chemical technique. Bull. Mater. Sci. 39, 177–186.

Rouchdi, M., Salmani, E., Hat, A.E., Hassanain, N., Mzerd, A., 2017. Synthesis and magnetic properties of Ni-doped ZnO thin films: experimental and ab initio study. Surf. Rev. Lett. 24, 1750085.

Saha, S.K., Rahman, M.A., Sarkar, M.R.H., Shahjahan, M., Khan, M.K.R., 2015. Effect of Co Doping on Structural, Optical, electrical and thermal properties of nanostructured ZnO thin films. J. Semiconduct. 36, 033004.

Shah, M.A.H., Khan, M.K.R., Karim, A.M.M.T., Rahman, M.M., Kamruzzaman, M., 2018. Fabrication of n-ZnO/p-Si (100) and n-ZnO:Al/p-Si (100) heterostructures and study of current-voltage, capacitance-voltage and room-temperature photoluminescence. J. Electron. Mater. 47, 879–886.

Tundermann, J.H., Tien, J.K., Howson, T.E., 2005. Nickel and nickel alloys. Kirk-Othmer Encyclop. Chem. Technol. 17 online edition.

Yildiz, A., Kayhan, B., Yurduguzel, B., Rambu, A.P., Iacomi, F., Simon, S., 2011. Ni doping effect on electrical conductivity of ZnO nanocrystalline thin films. J. Mater. Sci. Mater. Electron. 22, 1473–1478.

Zeng, H., Duan, G., Li, Y., Yang, S., Xu, X., Cai, W., 2010. Blue luminescence of ZnO nanoparticles based on non-equilibrium processes: defect origins and emission controls. Adv. Funct. Mater. 20, 561–572.

Zhang, Z., Ning, Y., Fang, X., 2019. From nanofibers to ordered ZnO/NiO heterojunction arrays for self-powered and transparent UV photodetectors. J. Mater. Chem. C. 7, 223–229.